TECHNICAL REPORT • OPEN ACCESS

Cryogenic characterization of Hamamatsu HWB MPPCs for the DUNE photon detection system

To cite this article: M. Andreotti *et al* 2024 *JINST* **19** T01007

Jinst

Published by IOP Publishing for Sissa Medialab

Received: *July 11, 2023*
Revised: *September 8, 2023*
Accepted: *November 16, 2023*
Published: *January 18, 2024*

TECHNICAL REPORT

Cryogenic characterization of Hamamatsu HWB MPPCs for the DUNE photon detection system

M. Andreotti,[f] S. Bertolucci,[l,e] A. Branca,[q,h] C. Brizzolari,[q,h] G. Brunetti,[q,h] R. Calabrese,[n,f] P. Carniti,[q,h] D. Casazza,[n,f] C. Cattadori,[h] E. Calvo,[b] A. Cervera,[d] S. Chiozzi,[h] V. Cicero,[l,e] A. Cotta Ramusino,[f] E. Cristaldo Morales,[q,h] C. Cuesta,[b] R. D'Amico,[n,f] A. De la Torre,[b] M. Delgado Gonzalez,[q,h] F. Di Capua,[r,i] D. Di Ferdinando,[e] A. Dyshkant,[k] M. Eads,[k] A. Falcone,[q,h] E. Fialova,[c] P. Filip,[j] G. Fiorillo,[r,i] M. Fiorini,[n,f] K. Francis,[k] F. Galizzi,[q,h] N. Gallice,[p,g] D. Garcia-Gamez,[o] M.Á. García-Peris,[d] T. Giammaria,[n,f] I. Gil-Botella,[b] C. Giugliano,[n,f] C. Gotti,[h] M. Guarise,[n,f] D. Guffanti,[q,h] M. Kovalcuk,[j] I. Lax,[e] M. Lazzaroni,[p,g] M. Lokajicek,[j] E. Luppi,[n,f] S. Manthey,[b] J. Martin-Albo,[d] N. Mauri,[l,e] L. Meazza,[q,h] A. Minotti,[q,h] N. Moggi,[l,e] E. Montagna,[l,e,*] A. Montanari,[e] I. Neri,[n,f] F.J. Nicolas-Arnaldos,[o] C. Palomares,[b] L. Pasqualini,[l,e] L. Patrizii,[e] L. Pérez-Molina,[b] G. Pessina,[h] V. Pia,[l,e] F. Poppi,[l,e] M. Pozzato,[e] M. Querol,[d] J. Rocabado,[d] A. Saadana,[d] P. Sala,[g] A. Sanchez-Castillo,[o] P. Sanchez-Lucas,[o] F.S. Schifano,[n,f] G. Sirri,[e] J. Smolik,[c] M. Spanu,[q,h] F. Terranova,[q,h] M. Tenti,[e] L. Tomassetti,[n,f] M. Torti,[h] N. Tosi,[e] A. Verdugo de Osa,[b] H. Vieira de Souza,[a,m,q] J. Zalesak,[j] B. Zamorano,[o] A. Zani,[g] S. Zucchelli,[l,e] J. Zuklin[j] and V. Zutshi[k]

[a] *APC, Laboratoire Astroparticule et Cosmologie, Université de Paris Cité, Paris, France*
[b] *CIEMAT, Centro de Investigaciones Energéticas, Medioambientales y Tecnológicas, E-28040 Madrid, Spain*
[c] *Czech Technical University, 115 19 Prague 1, Czech Republic*
[d] *Instituto de Física Corpuscular, Catedratico Jose Beltran, 2 E-46980 Paterna (Valencia), Spain*
[e] *Istituto Nazionale di Fisica Nucleare, Sezione di Bologna, 40127 Bologna, Italy*
[f] *Istituto Nazionale di Fisica Nucleare, Sezione di Ferrara, I-44122 Ferrara, Italy*
[g] *Istituto Nazionale di Fisica Nucleare, Sezione di Milano, 20133 Milan, Italy*

[*] Corresponding author.

https://doi.org/10.1088/1748-0221/19/01/T01007

2024 JINST 19 T01007

[h] *Istituto Nazionale di Fisica Nucleare, Sezione Milano Bicocca, 20126 Milan, Italy*
[i] *Istituto Nazionale di Fisica Nucleare, Sezione di Napoli, Naples, Italy*
[j] *Institute of Physics, Czech Academy of Sciences, 182 00 Prague 8, Czech Republic*
[k] *Department of Physics, Northern Illinois University, 1425 W. Lincoln Hwy., DeKalb, IL 60115, U.S.A.*
[l] *Dipartimento di Fisica, Università di Bologna, 40127 Bologna, Italy*
[m] *Universidade Estadual de Campinas, Campinas, SP, 13083-970, Brazil*
[n] *Università degli Studi di Ferrara, 44122 Ferrara, Italy*
[o] *University of Granada & CAFPE, Campus Fuentenueva (Edif. Mecenas), 18002 Granada, Spain*
[p] *Dipartimento di Fisica, Università degli Studi di Milano, Via Celoria, 16, 20133 Milan, Italy*
[q] *Dipartimento di Fisica, Università di Milano Bicocca, Piazza della Scienza, 3, 20126 Milan, Italy*
[r] *Università degli Studi di Napoli Federico II, Corso Umberto I 40, 80138 Naples, Italy*

E-mail: elisabetta.montagna@bo.infn.it

Abstract: The Deep Underground Neutrino Experiment (DUNE) is a next generation experiment aimed to study neutrino oscillation. Its long-baseline configuration will exploit a Near Detector (ND) and a Far Detector (FD) located at a distance of $\sim$ 1300 km. The FD will consist of four Liquid Argon Time Projection Chamber (LAr TPC) modules. A Photon Detection System (PDS) will be used to detect the scintillation light produced inside the detector after neutrino interactions. The PDS will be based on light collectors coupled to Silicon Photomultipliers (SiPMs). Different photosensor technologies have been proposed and produced in order to identify the best samples to fullfill the experiment requirements. In this paper, we present the procedure and results of a validation campaign for the Hole Wire Bonding (HWB) MPPCs samples produced by Hamamatsu Photonics K.K. (HPK) for the DUNE experiment, referring to them as 'SiPMs'. The protocol for a characterization at cryogenic temperature (77 K) is reported. We present the down-selection criteria and the results obtained during the selection campaign undertaken, along with a study of the main sources of noise of the SiPMs including the investigation of a newly observed phenomenon in this field.

Keywords: Cryogenic detectors; Photon detectors for UV, visible and IR photons (solid-state); Photon detectors for UV, visible and IR photons (solid-state) (PIN diodes, APDs, Si-PMTs, G-APDs, CCDs, EBCCDs, EMCCDs, CMOS imagers, etc)

2024 JINST 19 T01007

Contents

2024 JINST 19 T01007

1 Introduction

DUNE (Deep Underground Neutrino Experiment) is a next-generation dual-site experiment for neutrino oscillation studies, which will carry out a detailed study of neutrino mixing employing high-intensity ν_μ and $\bar{\nu}_\mu$ beams measured over a long baseline [1]. The DUNE Far Detector (FD) will consist of four liquid argon time projection chambers (LAr TPC) with a total mass of nearly 70 kt (fiducial mass of at least 40 kt). The first module, will be a LAr TPC with Horizontal Drift configuration (FD1-HD). This liquid argon (LAr) technology will make possible the reconstruction of neutrino interactions with image-like precision. In addition, argon produces scintillation light peaked at 127 nm [2]. The collection of this prompt signal, thanks to a Photon Detection System (PDS), provides an initial start time for every event, and its efficient detection can enhance DUNE detector capabilities, mainly for non-beam and low-energy physics. The design of the four identically sized modules is sufficiently flexible for staging construction and evolving the LAr TPC technology.

The PDS detects the Vacuum Ultra Violet (VUV) scintillation light produced by ionizing tracks in the TPC and operates in Liquid Argon. The light collector modules, the so-called X-ARAPUCAs [3], proposed for DUNE Far Detector, are based on the concept of photon trapping inside a highly reflective box using a wavelength shifting (WLS) bar, so that photons can be detected with Silicon Photomultiplier (SiPM) arrays. The side facing the active volume of the detector is covered by

dichroic filters with a sharp cut-off at 400 nm and with an outer layer of p-Terphenyl (pTP) that converts the incident 127 nm scintillation photons into 350 nm wavelength. Then the light reaches the WLS bar and it is shifted to the visible range (430 nm). The WLS re-emitted light can be trapped by total internal reflection or escape and be reflected on the dichroic filter, reaching at the end the SiPM photosensors. This design can be tailored to fit the different geometric necessities of each FD module.

In order to validate the DUNE technology, prototypes are being designed, built and tested at CERN, the so-called ProtoDUNEs [1, 4]. ProtoDUNE-HD will test the final design of the LAr TPC Horizontal Drift (HD) detector components at a scale of 1:1 in 2023. In particular, the X-ARAPUCAs of the HD module will be tested for the first time. The so-called X-ARAPUCA SuperCell is composed by six $10\times10\,\mathrm{cm}^2$ pTP-coated dichroic filters, a 60 cm WLS bar and 48 SiPMs ganged all in parallel at the input of a cold amplifier. Four of these SuperCells are used to assemble a full optical module, with $2\,\mathrm{m}\times12\,\mathrm{cm}$ approximate dimensions, that is eventually embedded in the anode planes.

The SiPMs for DUNE are custom products by two vendors: Fondazione Bruno Kessler (FBK) and Hamamatsu Photonics K.K. (HPK), specifically designed for being used at cryogenics temperatures. The 2.5 years R&D carried out with the DUNE Photon Detection System (PDS) Consortium has resulted in the development of several prototypes addressing DUNE technical requirements.

In this paper we show the features of the four SiPM prototypes developed by HPK, the down-selection criteria, and the outcome of the down-selection procedure. The selection procedure is based on tests carried out with a small-size production batch (25 SiPMs batch) to measure their performance. A complete characterization was performed with a batch of 250 SiPMs per model to validate the thermal performance for a statistically significant set of SiPMs. All these tests were done in dedicated test-benches arranged at seven different institutes of the PDS Consortium: *CIEMAT, Centro de Investigaciones Energéticas, Medioambientales y Tecnológicas*, in Madrid; *Istituto Nazionale di Fisica Nucleare* and *Università di Bologna*, in Bologna; *Istituto Nazionale di Fisica Nucleare* and *Università di Ferrara* in Ferrara; *Istituto Nazionale di Fisica Nucleare* and *Università di Milano-Bicocca* in Milano; *Institute of Physics, Czech Academy of Sciences* in Prague; *Instituto de Física Corpuscular*, in Valencia and the *Northern Illinois University, Department of Physics*.

2 SiPM requirements

The DUNE PDS and SiPMs general requirements directly follow from the DUNE Physics Requirements [5] and are summarized as follows:

- The SiPM Photon Detection Efficiency (PDE) in the wavelength range of photons emitted by compatible wavelength-shifters (peak wavelength 430 nm) should be at least as good as commercial devices such as Hamamatsu S13360 i.e. > 35% at 430 nm.
- SiPM dimensions should be compatible with the mechanical design of the X-ARAPUCA module.
- The SiPM characteristics (along with the associated front-end electronics) should allow for single photo-electron (p.e.) identification for detection of low-energy neutrinos interacting far from the X-ARAPUCA module (in the vicinity of the Cathode Plane Assembly) and for

2024 JINST 19 T01007

Table 1. Specific requirements for the SiPMs of the FD1-HD photon detection system.

Parameter	Value	Note
SiPM dimension and packaging	$6 \times 6\,\mathrm{mm}^2$, SMT (Surface Mount Technology)	Compatible with the PDS module final design
Cell pitch	50–150 µm	As large as possible in the range allowed
PDE at nominal voltage (Vop)	> 35% at 430 nm	At room temperature
Window material	Siliconic or epoxidic	Cryogenic reliable
DCR	$< 200\,\mathrm{mHz/mm}^2$ at Vop	At 77 K
Cross-talk probability	< 35% at Vop	At 77 K
After-pulsing probability	< 5% at Vop	At 77 K
Gain	$2 \text{ to } 8 \cdot 10^6$	Not critical
SiPM recovery time	200–1000 ns	Optimal for cold electronics
Breakdown voltage (Vbd) spread	< 200 mV (max-min)	Per group of 240 SiPMs (one PDS module)
Maximum Vbd voltage spread	< 2 V (max-min)	Global spread
Thermal cycles	> 20	Tested at 77 K by the Consortium
Signal to noise ratio in ganging	> 4	ganging of 48 SiPMs (1 DAQ channel)

reliable calibration and threshold setting. Particularizing, the PDS must have a signal to noise ratio larger than 4 for single acquisition channel.

- For a given threshold, the Dark Count Rate (DCR) of the SiPM at LAr temperature should not dominate that generated by radiological decays of the Argon or other impurities in the liquid.
- The SiPMs should be able to meet the previous requirements and function within specifications for at least 10 years in a LAr environment.

Specific requirements are the technical characteristics of SiPMs that meet the requirements above (reported in table 1). Since the long time exposure cannot be tested intrinsically in the laboratory, the sensors are exposed to several controlled cryogenic cycles so that it can be veryified they are not damaged due to thermal stress.

In 2020–2021 HPK produced four prototypes to assess the DUNE requirements and improve the performance with respect to commercially available products. These prototypes characteristics are shown in table 2.

3 Experimental setup and measurement procedure

As previously mentioned, seven laboratories were involved in the SiPMs characterization tests. During the test campaign, it was crucial to ensure that at least two laboratories tested the same

2024 JINST 19 T01007

Table 2. Different SiPMs prototypes produced by HPK.

Model	Characteristics	Notes
HPK S13360-9932 50 µm-LQR	Cell pitch 50 µm, low quenching resistance (280 kΩ) at 77 K	Standard quenching and cell pitch
HPK S13360-9933 50 µm-HQR	Cell pitch 50 µm, high quenching resistance (660 kΩ) at 77 K	High-R quenching and standard cell pitch to reduce the impact of after-pulsing and possibly dark current and cross-talk
HPK S13360-9934 75 µm-LQR	Cell pitch 75 µm, low quenching resistance (280 kΩ) at 77 K	Standard quenching and large cell pitch to increase fill factor (active area/total area)
HPK S13360-9935 75 µm-HQR	Cell pitch 75 µm, high quenching resistance (660 kΩ) at 77 K	High-R quenching and large cell pitch to reduce the impact of after-pulsing and possibly dark current and cross-talk, and increase fill factor

model of SiPM and compared the results. The measurements of each model performed by different laboratories resulted to be consistent. A description of the experimental facilities and equipment used for the measurements is provided in this section.

Description of the setups. In order to have compatible measurements in the various laboratories, it is important to have test setups with same specifications. All of them consist of: a small dewar filled with liquid nitrogen (LN2), a movable black box containing the sensors and a preamplifier used for the measurements (figure 1). The data acquisition is done either with an oscilloscope or an ADC. A description of a general setup is reported in the following as an example (figure 3). All the laboratories have chosen similar solutions with same requirements.

The system is composed of a small dewar (~ 5 liters volume) which can be filled with LN2. The top aperture of the dewar can be closed with a black plastic plug. The plug can be manually moved up and down through a mechanical system. Power and signal cables go inside the dewar through holes drilled in the plug where the light tightness is guaranteed by black silicone or putty. For the measurements a preamplifier and the device under test are mounted inside a metallic box attached to the plug with a holder. The box helps in shielding the electromagnetic noise picked up by the amplifier and also the Cherenkov light produced by cosmic rays inside the volume of the dewar that would spoil the intrinsic Dark Count Rate (DCR) measurement. The amplifier used was the one developed at the Milano-Bicocca University [6]. Few setups used a similar amplifier with analogous characteristics. For the DCR measurements, the output of the preamplifier is connected to the input of a digital scope for the data taking. A second stage warm amplifier may be needed if the sensitivity of the oscilloscope is not enough. The waveforms are analysed offline. For a successful measurement of the very low DCR it is important to ensure the light tightness of the plug. Hosting the test system in a dark room helps in shielding the dewar to external light. The current-voltage characteristics (I-V curves) are measured by connecting the device under test directly to a source meter. The relevant specifications of the instrumentation are summarized in table 3.

2024 JINST 19 T01007

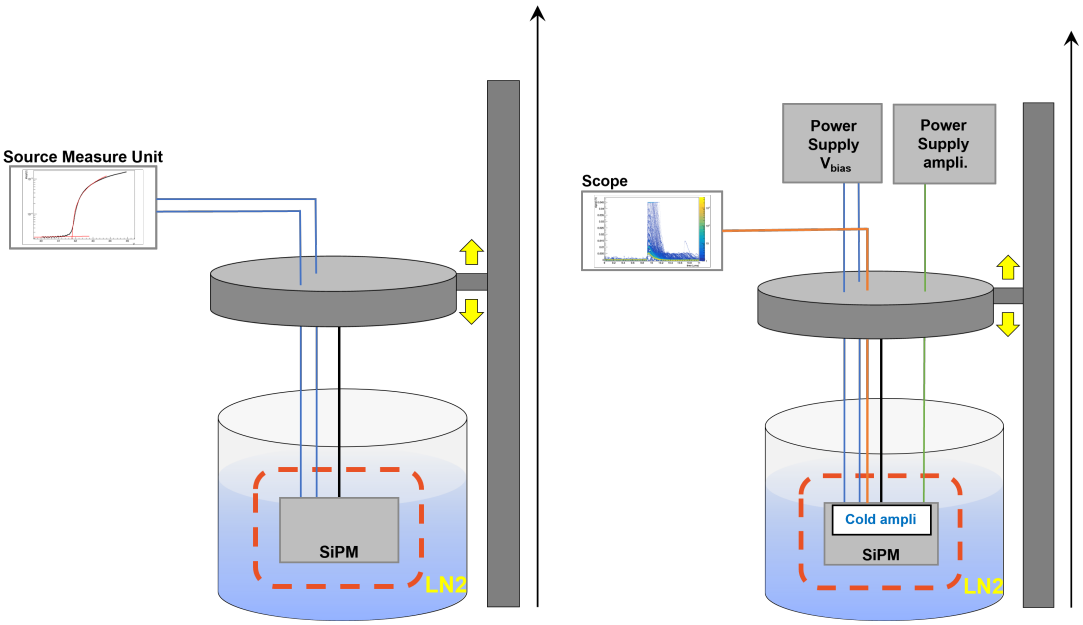

Figure 1. Setup for the measurements. On the left the apparatus used for the I-V measurements, on the right the setup for the DCR and gain measurements.

Two batches of each SiPM model (table 2) have been tested: a first batch of 25 SiPMs tested individually (figure 2, top) and a second batch of 250 SiPMs, mounted in group of 6-sensors per PCB (Printed Circuit Board) as designed for the final configuration of the Photon Detection System (figure 2, bottom).

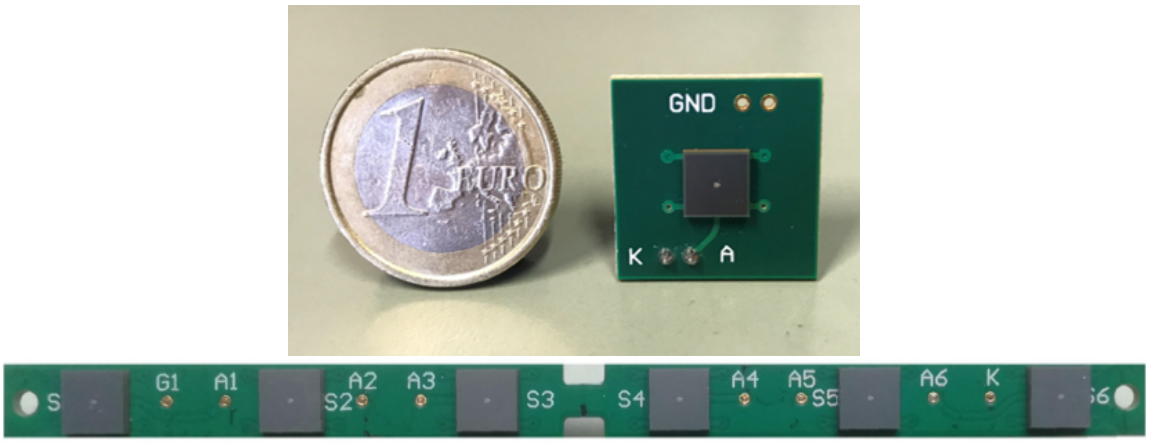

Figure 2. Top: single SiPM from the first batch of 25 samples per model. Bottom: array of 6 SiPMs mounted on a PCB with common cathode and single anode per each sensor as in the final design for DUNE FD1-HD.

Testing procedure of single sensors. The characterization of the sensors at the level of single SiPMs follows a standard procedure. Some preliminary tests at room temperature were performed before the first cool down in LN2 to validate the information provided by the vendors. The I-V

2024 JINST 19 T01007

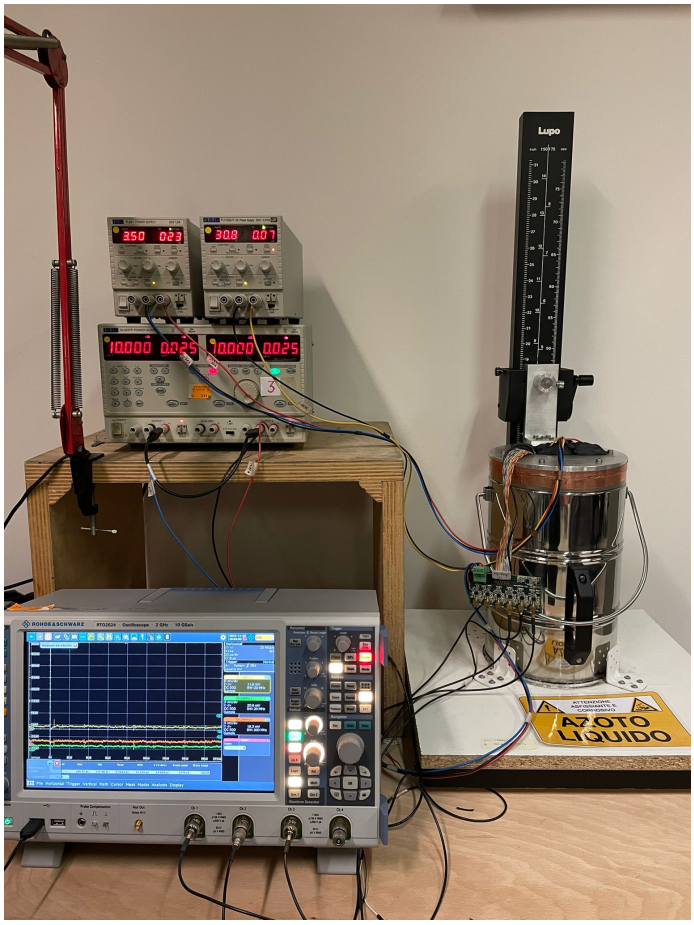

Figure 3. Example of the experimental setup used for the measurements. On the right, the dewar filled with liquid nitrogen where the samples are allocated; on the left, the scope used for the DCR measurements and the power supplies for the amplifier.

Table 3. Relevant specifications of instrumentation used for the measurements.

Device	Specifications
Scope	1 GHz bandwidth, 5 Gs/s, 8 bit vertical scale, 10 Msample memory
Source Measure Unit (SMU)	0–100 V voltage range, few pA precision
Source meter cable	less than few pA loss

characteristics in forward and reverse bias were measured for all the sensors of the 25-batch in order to measure the breakdown voltage and the quenching resistance and compare them to the data from the vendor. Then, the measurements at 77 K were performed. The sensor fulfills the DUNE specifications if it can withstand more than 20 thermal cycles. It means that the response of the SiPM in terms of reverse I-V curve and single p.e. amplitude at fixed over-voltage (OV) does not change after the cycles. Such an assessment must be done at 77 K before and after the cycling. The most critical item is the cool-down of the sensor because a damage due to a fast cooling cannot be

2024 JINST 19 T01007

uniquely attributed to a sensor out of thermal specs or to a failure due to excessive thermal gradients. The thermal cycle is composed of three phases: exposing the sensor to LN2 vapors for ∼8 minutes, submerging the sensor in LN2 for ∼11 minutes, exposing the sensor to LN2 vapors for ∼ 8 minutes, warming up at room temperature until it thermalizes to the temperature of the lab (figure 4).

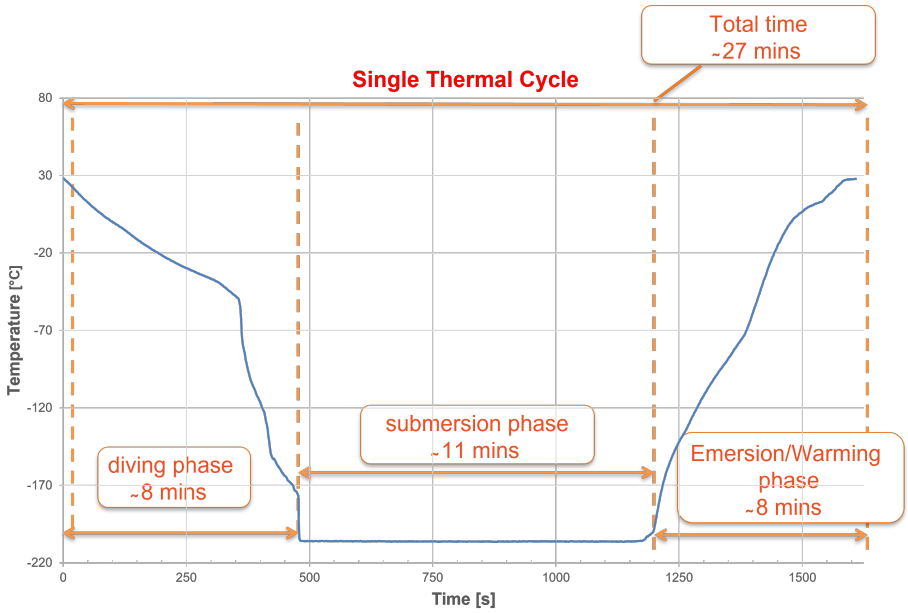

Figure 4. Temperature profile as a function of the time for a single thermal cycle. The different phases are shown with their corresponding duration along with the total time for one cycle.

All tests at cold have been performed after a total thermalization period of 11 minutes. A platinum resistance termometer (PT100) in thermal contact with the amplifier was used to cross-check the thermalization time and demonstrate that the apparatus was able to keep a stable temperature during the entire duration of the tests. All measurements, except DCR measurements that are time consuming, should be performed (at least) twice: at the first cool down and at the 20th cool down. The results taken at the 20th cool down will be labeled as "final" for that sensor.

The sequence for the characterization tests at 77 K is the following:

- I-V curve in forward bias. We use a semiconductor analyser to speed up the measurement or, equivalently, an apparatus able to achieve a precision < 1 nA. The measurement is aimed at providing a direct estimate of the quenching resistance with a precision better than 10%.
- I-V curve in reverse bias. Again, a semiconductor analyser is the most convenient choice. Otherwise a standard Source Measure Unit (SMU) can be used at the expenses of an increased dead time among measurements. The measurement provides the breakdown voltage and the useful over-voltage range. We define the breakdown voltage as the maximum of $I^{-1}\frac{dI}{dV}$. The measurement of the breakdown is eased if the sensor is illuminated by a faint LED or laser whose wavelength is in the visible or near-UV.
- Gain of the sensor. The measurement is performed as a function of the OV in the range of interest for DUNE. We recorded and integrated the photoelectron (p.e.) amplitudes after

2024 JINST 19 T01007

illuminating with a LED source and test the linearity of the response and the relative gain (charge per p.e.). We also performed an absolute gain measurement after calibrating the response function of the cold amplifier.

- Primary Dark Count Rate (DCR). Rates below 100 mHz/mm^2 at the 0.5 p.e. threshold are expected. As a consequence, light screening and electronic noise reduction is particularly challenging and may require a dedicated dark room. The DCR is measured as a function of the over-voltage in the range of interest for DUNE.

- Correlated noise (cross-talk and after-pulse). In order to evaluate correlated noise for a given OV, we acquired dark noise triggering at 0.5 p.e. threshold and recorded the absolute time of the waveform. Correlated noise can be extracted by analyzing the amplitude as a function of the absolute time scale of the recorded signals. Note that DCR and correlated noise can be extracted by the same dataset if triggering at 0.5 p.e. threshold is feasible.

Gain, DCR and correlated noise measurements are characterized at three different Photon Detection Efficiencies (PDEs): 40%, 45% and 50%, corresponding to +3, 4 and 5 V of OV for 50 µm-pitch SiPMs, and to +2, 2.5 and 3 V of OV for 75 µm-pitch SiPMs. This relation is given by the vendor, and the measurement of the breakdown voltage allows to set the appropriate OV for each sensor. The PDE is defined as the ratio between detected photons and the number of incident photons. It is calculated as the product of the quantum efficiency, that is the probability that carriers are generated by light incident on a pixel; the fill factor, which is the ratio of active to total area of the SiPM; and the avalanche probability, that is the probability that charge carriers generated by the photon cause a multiplication avalanche.

Testing procedure of SiPMs on the boards The tested boards are identical to the final boards for ProtoDUNE-HD and, hence, they host 6 SiPMs per board. These arrays have an output connection for each SiPM allowing for the individual test.

The measurements performed for these samples are the following:

- a preliminary measurement of I-V curve at room temperature in forward and reverse bias for all the boards to validate the information from the vendor;

- reliability at cryogenic temperature. This test is done following the same procedure used for the 25-batch and aims to verify the integrity of the 6-SiPM board and its components;

- I-V curve at 77 K in forward and reverse bias for each SiPM on the boards for each model, following the same procedure as for the 25 sensor batch. Comparing I-V results before and after thermal cycles in order to check that they did not affect the SiPMs;

- characterization of the gain, DCR and correlated noise of a 10% of the SiPMs of each model for the downselection.

2024 JINST 19 T01007

4 Experimental results

4.1 Reliability to cryogenic cycles

As previously explained, all SiPMs from both batches were exposed to several cryogenic cycles. In the case of the 25-batch, all tested SiPMs were completely characterized before and after the cycling in order to study any possible effect in the different parameters of the sensors. After this process, every studied sensor of the first batch fulfilled DUNE requirements before and after the thermal cycles, being both sets of measurements compatibles within the experimental uncertainty.

This was repeated afterwards for the SiPMs of the second batch. However, in this case, only the breakdown voltage and the quenching resistance were measured before and after the cycling. No significant difference was detected either.

In the following sections, for simplicity, only the results from the second batch (the one formed by 6-SiPMs arrays) will be shown, since they were the ones used for the down-selection. Even though a total number of 1000 sensors was received, 95% of them were tested. From the 250 SiPMs provided of each model, 41 6-SiPMs boards were prepared, meaning that four SiPMs of each model were not used for the tests. From the 164 boards, 22 were used for SuperCell testing [7], thus not appearing in the following results.

4.2 I-V curves, V_{bd}, R_q

The breakdown voltage and the quenching resistance of each SiPM are extracted from the I-V curves. The vendor provided these values at room temperature, therefore measurements at room temperature were mainly performed as a crosscheck for the experimental setups of the different laboratories. Additional measurements at LN2 temperature were done to characterize the SiPMs at cryogenic condition.

It can be seen in the top part of the figure 5 an example of a reverse biased I-V curve of a SiPM, in which the current grows as a function of the bias voltage. In the bottom of the same plot the curve $\frac{dI}{IdV}$, also known as variation rate, is presented. The maximum of this curve corresponds to the breakdown voltage of the sensor.

The breakdown voltage of the SiPMs was measured at room temperature, and a comparison with the data provided by the vendor is shown in figure 6, left. It can be seen that both distributions have a similar shape and standard deviation. The small shift in the mean (0.2%) is due to the different method used by the vendor to determine the breakdown voltage: from the Gain vs Voltage curve, the breakdown voltage can be estimated as the voltage that corresponds to a zero gain. It can also be observed the existence of two populations. This effect is present in every model and in the information provided by the vendor.

The breakdown voltage measurements were repeated at LN2 temperature and they are presented in figure 6, right. A decrease on the values of about 10 V can be observed, as expected, while the shape of the distribution remains approximately the same. It is known there is a linear relation between the breakdown voltage of SiPMs and temperature for small temperature variations, but this observation suggests that a strong correlation is also present even for very large temperature variations.

The quenching resistance of the SiPMs is obtained by fitting the I-V curve measured in forward bias. When a forward bias is applied, the SiPM does act as a diode in series with the quenching resistor. When the diode becomes conductive, the drop in current is negligible with respect to the drop

2024 JINST 19 T01007

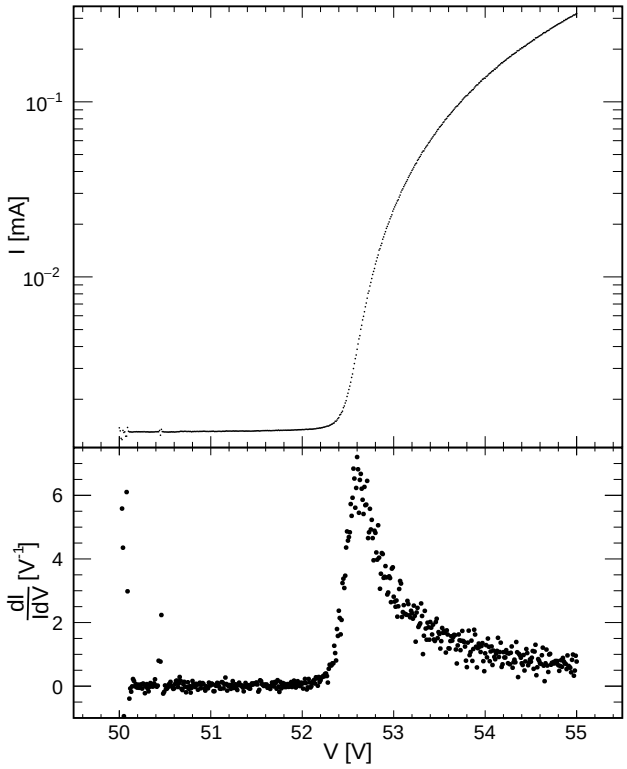

Figure 5. Top: I-V curve in reverse bias. The sudden change on the current corresponds to the voltage in which the SiPM starts functioning in geiger mode. Bottom: variation rate of the plot above. The maximum of this curve corresponds to the value of breakdown voltage.

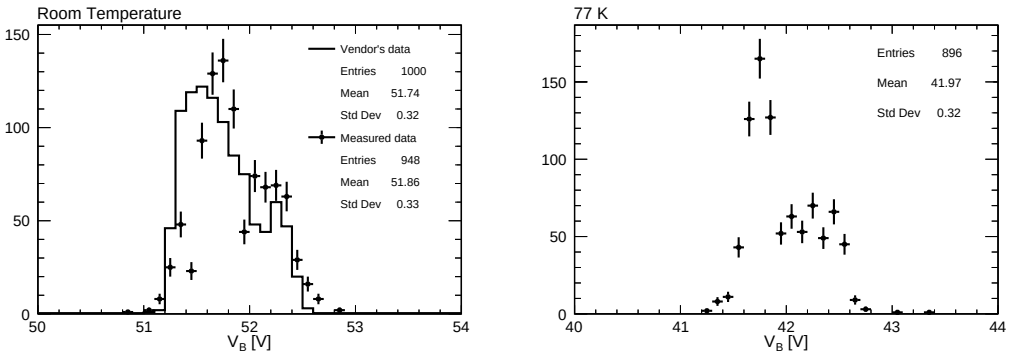

Figure 6. Left: breakdown voltage comparison between vendor's data (histogram) and our measurements (black points) for the 250-batch at room temperature. Right: breakdown voltage measured at LN temperature (no information from the vendor). The bin width is 0.1 V, the approximate resolution of the measurement. There are more room measurements because some of the SiPM used for SC tests were characterized at room temperature before they were selected for these tests.

2024 JINST 19 T01007

generated by the resistor, so the measured current as a function of the voltage is inversely proportional to the equivalent quenching resistance of the SiPM (figure 7, left). The range of the fit was chosen to be between 5.2 and 6.0 mA to match the data provided by the manufacturer (figure 7, right).

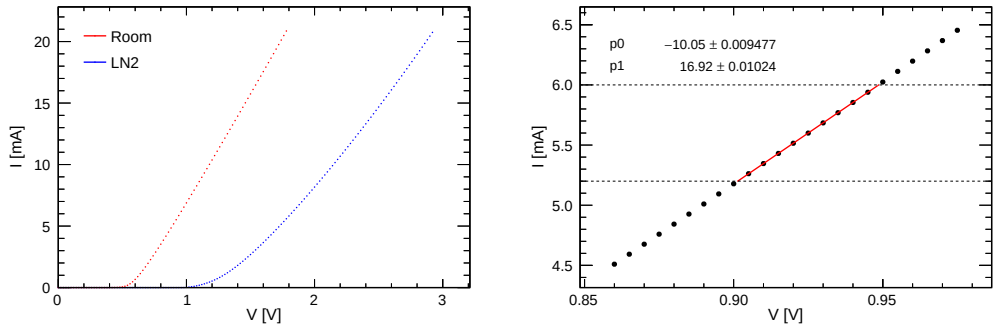

Figure 7. Left: I-V curves in forward bias at room and liquid nitrogen (LN2) temperature. The observed difference is due to the increase of the resistance at cryogenic conditions. Right: linear fit for the curve at room temperature, $I = p0 + p1 \cdot V$. The SiPM quenching resistance is obtained from the inverse slope of the fitted function.

In figure 8 the quenching resistance measurements at room temperature are presented and compared with the data provided by the vendor. It is important to note here that the vendor provided the measurement for a single sensor of the batch. Because of that, as in the case of the breakdown voltage, only a qualitative comparison can be done: the results provided by the different laboratories are coherent between themselves and with the value provided by the vendor.

4.3 Gain

When a photon is detected by the SiPM the absolute charge released by the sensor (the gain) is obtained by integrating the waveform generated and multiplying by the amplification factor of electronic boards. The charge distribution can be fitted to a sum of gaussian distributions (see figure 9). The difference between the mean value of the single photoelectron peak and the pedestal is considered to be the gain of the SiPM.

In figure 10 the different gains measured for each SiPM model are presented. As expected, the models with larger cell pitch have a larger gain for the same PDE value.

4.4 Dark Count Rate

Based on the data provided by the vendor, the rate of signals above the half photoelectron level (DCR) at room temperature of the SiPMs is expected to be between 2 and 6 MHz. Based on previous studies [8–10], DCR was expected to decrease down to Hz — even mHz — per mm^2 scale at LN2 temperature.

Shortly after tests started, an unexpected behaviour in DCR measurements was observed. Instead of obtaining larger rates as OV increased, measured values fluctuated randomly. In figure 11 the DCR measurements of six SiPMs of the same model (characterized in the same laboratory) are presented. It can be seen how DCR does not increase with PDE (OV), as it would be expected. Instead, it seems to fluctuate around a mean value.

2024 JINST 19 T01007

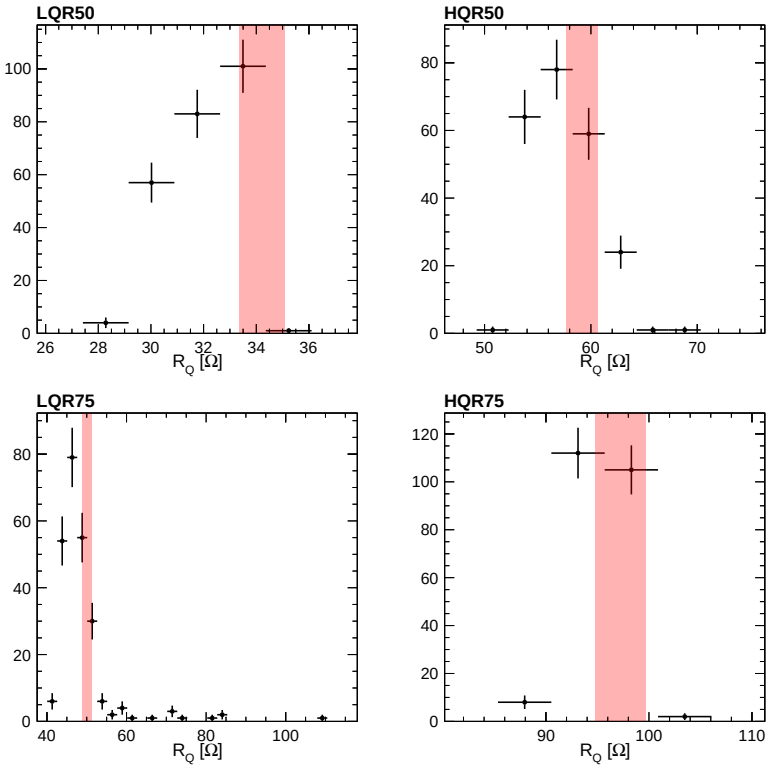

Figure 8. Equivalent resistance for the 250-batch SiPM measured at room temperature for the different SiPM models. The binning of the histogram corresponds to the error of the measurements, that was estimated to be around 5%. Red band represents vendor measurement with the associated systematic uncertainty, which is also 5%.

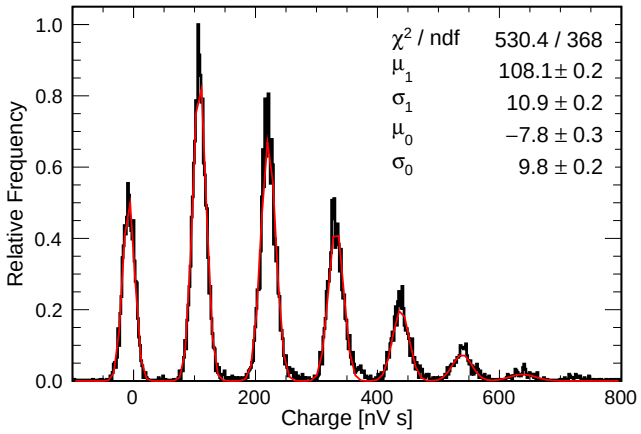

Figure 9. Charge distribution for a given sensor. It is illuminated with an LED, and the event waveforms are integrated to generate this histogram. The first peak corresponds to the pedestal, i.e., no photoelectrons are detected; the second peak corresponds to the detection of a single p.e., the third to two p.e. detected simultaneously; and so on. The distribution is fitted to a sum of gaussian distributions, and the difference between the fitted mean of the single p.e. peak (μ_1) and the fitted mean of the pedestal (μ_0) is considered to be the gain of the sensor.

2024 JINST 19 T01007

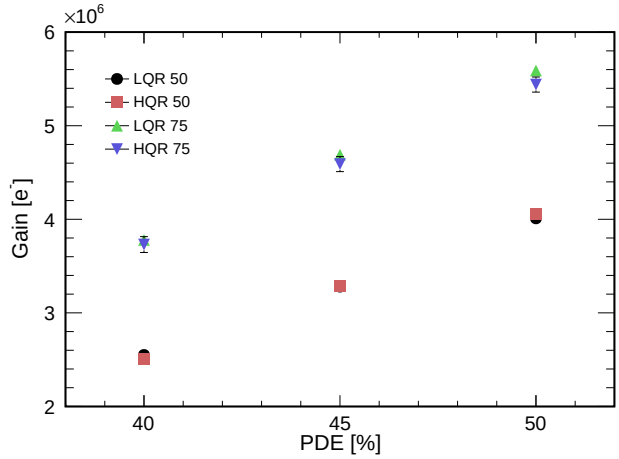

Figure 10. Average gain measured for each SiPM model. The error bar represents the standard deviation. A good linearity with the PDE is observed.

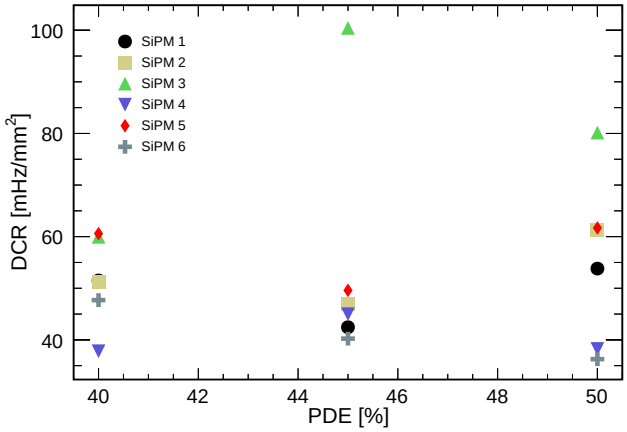

Figure 11. DCR measured for six different SiPMs of the same model in cryogenic conditions. None of them seems to follow a clear relation with the PDE — bias voltage. The error associated to these data points is statistical.

It was soon realized that measured DCR had two different components: the standard DCR (the goal of the measurement) and an additional 'burst' component. The so-called burst phenomenon was observed to be anticipated by a very large pulse (even of hundreds of photoelectrons) followed by hundreds of single photoelectrons with a time separation of the order of ms (figure 12).

This burst phenomenon, which will be analyzed in detail in the following section, was found out to be random and similar in the four SiPM models provided by the vendor. For this reason, the burst component of the DCR was subtracted in the offline analysis and only the standard uncorrelated component of the DCR was considered for the down-selection. It can be seen in figure 13 the results obtained for each model. Although the error bar is quite big, mainly due to the fluctuations from sensor to sensor, and the possible different measurement sensitivities of the involved laboratories, it can be seen that all models fulfill the DCR requirement. We noted that models with smaller pitch present a lower DCR.

2024 JINST 19 T01007

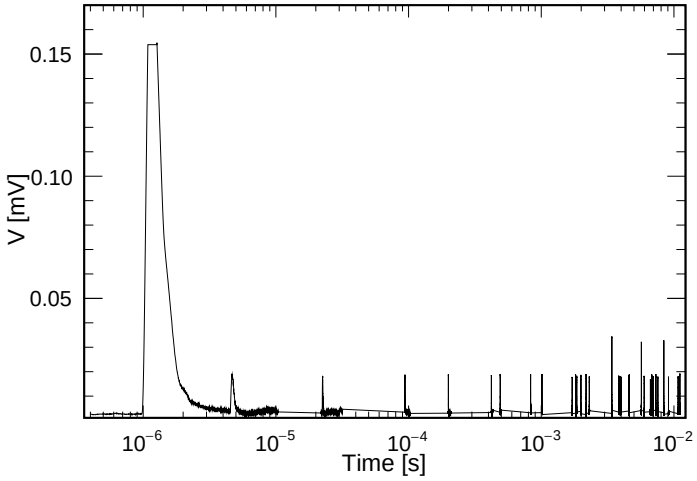

Figure 12. Example of the burst phenomenon observed. Figure shows the temporal signal trace of the bursts pulses anticipated by a large pulse with amplitude of several photoelectrons.

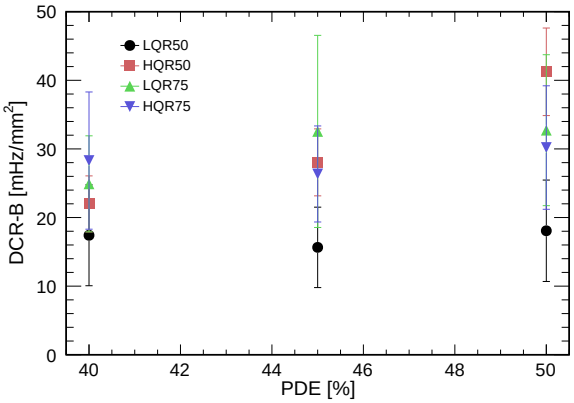

PDE	DCR (mHz/mm^2)			
	LQR50	HQR50	LQR75	HQR75
40	17 ± 7	22 ± 4	25 ± 7	28 ± 10
45	16 ± 6	28 ± 5	33 ± 14	26 ± 7
50	18 ± 7	41 ± 6	33 ± 11	30 ± 9

Figure 13. Averaged DCR after burst subtraction per SiPM model. As before, the error represents the standard deviation among measurements.

4.5 Correlated noise

Correlated noise involves cross-talk (XT) probability and after-pulse (AP) probability. The cross-talk makes reference to optical cross-talk: when a cell of a SiPM fires, accelerated carriers in the avalanche can emit photons. These photons can propagate to neighbouring cells and trigger further avalanches with a negligible time difference, producing a multiple p.e. output signal when instead only one real photon was detected. On the other hand, the after-pulse phenomenon is caused by the presence of impurities in the SiPM cells. When a p.e. is detected, some electrons of the avalanche can be trapped by impurities inside the Silicon crystal lattice. If the trapped part is released after the reset time of the cell, a secondary spurious pulse is generated. This could be misinterpreted as a single p.e. signal. A high quenching resistance in the sensor could possibly reduce the impact of the phenomenon by extending the recovery time of the SiPM: since the sensor is not sensitive during its recovery time,

2024 JINST 19 T01007

the charge of the delayed signal is not collected, i.e. the photon counting resolution of the sensor is less affected by after-pulsing. Same reasoning applies to the possibility of decreasing DCR and XT.

Correlated noises are obtained from the same measurement as the DCR.

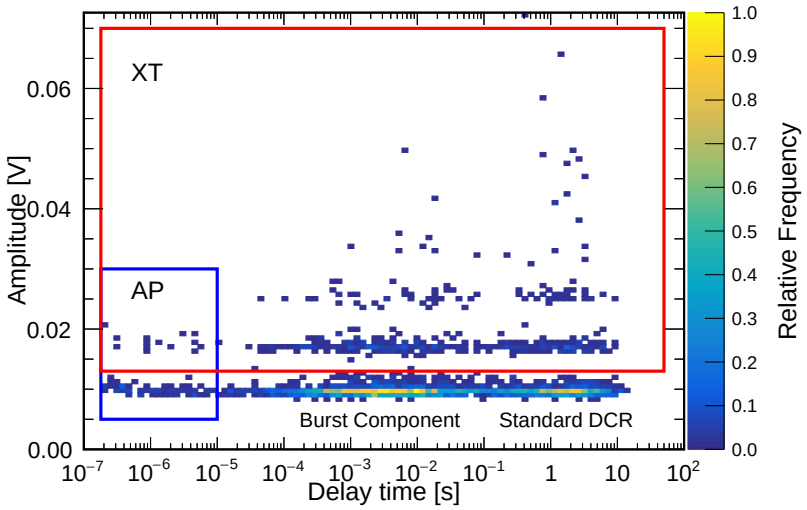

Figure 14. Pulse amplitude versus delay time with respect to previous event. The blue rectangle in the bottom left of the plot represent the events contributing to the AP, and the bigger rectangle represents the events contributing to the XT. The color map allows to differentiate between the burst component in the region of the milliseconds, and the standard DCR in the region of the seconds.

In figure 14, the amplitude of each pulse is presented against the delay time with respect to the previous pulse. The cluster of points around 0.01 V corresponds to the single photoelectron level, the one around 0.015 V to the two photoelectron level, and so on. On one hand, the XT probability is defined as the number of events above 1.5 photoelectrons divided by the total number of events. On the other hand, the AP probability was defined as the number of pulses with a time delay below 5 µs divided by the total number of pulses. This time delay interval has been set accordingly to the DAQ requirements envised for the PDS in DUNE.

Results for cross-talk and after-pulse measurements are presented in figure 15 averaged by model.

4.6 Unexpected observation of bursts of signals

The presence of an unexpected phenomenon in the dark current evaluation has been observed during the DCR measurements at liquid nitrogen temperature. Beyond the usual uncorrelated single events (signals with amplitude larger than 0.5 Single Photoelectron or SPE) that happen at ~Hz rate, random bunches of consecutive signals have been observed at a rate about 100 times larger (figure 12). These trains of signals have been denoted as bursts of events [11]. As shown in figure 16, which represents the distribution of the time-interval (Δt) between two consecutive events for the SiPM, this anomalous behaviour results in a non-flat trend. We can clearly identify periods in which events are separated by time intervals of the order of seconds, whereas we can also identify other periods in which events are separated by ms. These trains of events separated by ms are known as burst events.

2024 JINST 19 T01007

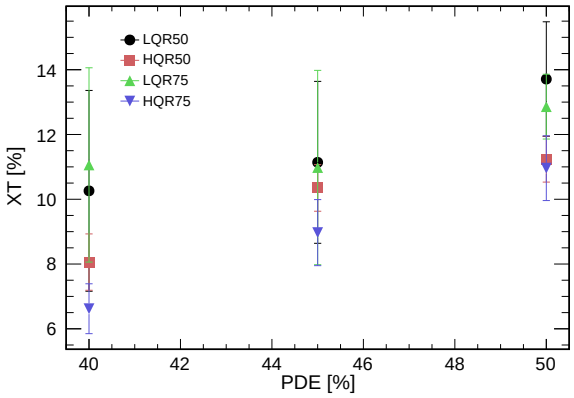

PDE	XT (%)			
	LQR50	HQR50	LQR75	HQR75
40	10 ± 3	8.1 ± 0.9	11 ± 3	6.6 ± 0.7
45	11 ± 3	10.4 ± 0.7	11.0 ± 0.3	9.0 ± 1.0
50	13.7 ± 1.8	11.2 ± 0.7	12.9 ± 1.0	11.0 ± 1.0

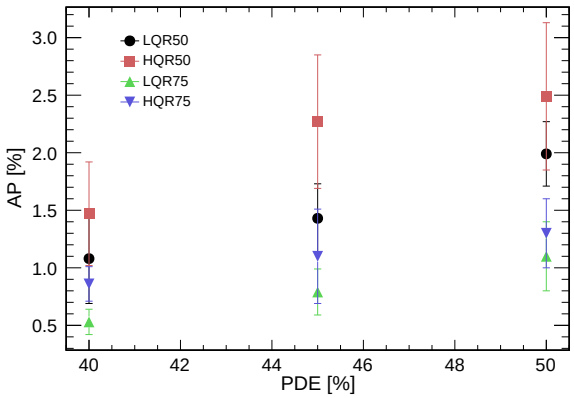

PDE	AP (%)			
	LQR50	HQR50	LQR75	HQR75
40	1.1 ± 0.5	1.5 ± 0.5	0.5 ± 0.2	0.9 ± 0.2
45	1.5 ± 0.3	2.3 ± 0.6	0.8 ± 0.2	1.1 ± 0.4
50	2.0 ± 0.6	2.5 ± 0.6	1.1 ± 0.3	1.3 ± 0.3

Figure 15. Top: cross-talk probability. Bottom: after-pulse probability. The error represents the standard deviation of the samples.

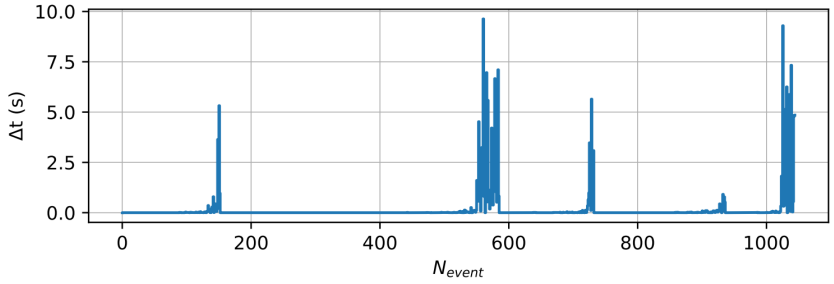

Figure 16. Time-interval (Δt) between two consecutive events (signals with amplitude larger than 0.5 Single Photoelectron or SPE) for the SiPM as a function of the event number.

These bursts of events are also identifiable in the 2-dimensional correlated noise plot as the one shown in figure 14. In this figure, a cluster of events with a SPE amplitude but a Δt of the order of ∼ [0.1–10] ms, is clearly distinguishable from the dark signals clusters of afterpulse, cross-talk and primary dark noise signals. Usually, in a single burst we can recognize hundreds of SPE amplitude signals separated by [0.1 − 10] ms Δt resulting thus in a length of few tenths of a second.

We observed the bursts in all the tested SiPM models, and the randomness of this behaviour brings the DCR to different values when repeating the measurement on the same SiPM. This

2024 JINST 19 T01007

randomness raised the need of a new bursts-independent parameter to compare the performances of different SiPM models in terms of dark noise ($DCR_{NoBursts}$). For this purpose, we developed two analysis tools to distinguish the burst contribution from the standard DCR. These two algorithms will be referred as the *tag* and the *fit* methods and will be discussed in the following paragraphs.

The *tag* method is used to isolate the burst's events one by one, in this way we can remove their contribution to the DCR value, and also study them in more detail. This method is based on finding consecutive events with short time-interval Δt between them, putting an upper limit to this delay Δt_{max}. In order to distinguish an event within a burst from an after pulse, the number of consecutive events N_{ev} must be larger than a certain threshold N_{min}, typically set to 5. A visual representation of these parameters is reported in figure 17. Best values for bursts identification were found by tuning these parameters to catch all bursts, checking on several sets of data, resulting in $\Delta t_{max} \sim 100$ ms, $N_{min} \sim 5$.

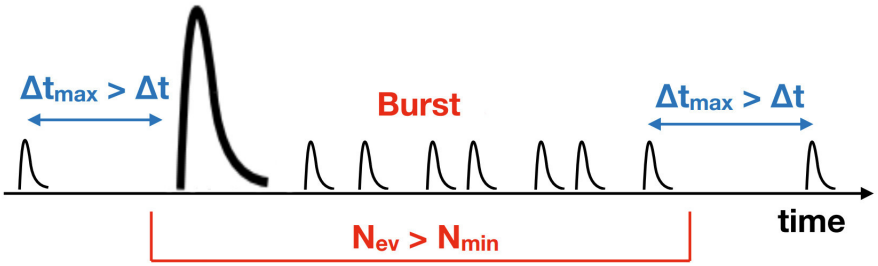

Figure 17. Sketch of a burst with its identification parameters.

The *fit* method also allows to identify the standard DCR cluster from the burst contribution in the Δt distribution, but is both conceptually and practically different. In fact, it relies on a fit of the histogram as shown, for example, in figure 18. The empirical functions used for the fit are a Poissonian distribution for the uncorrelated DCR, performed in the time interval $\Delta t = [0.1\text{–}100]$ s, and an over-dispersed Poissonian in the interval $\Delta t = [10^{-5} - 10^{-1}]$ s for the burst contribution.

In order to cross-check the validity of the two methods, we compared the results in terms of DCR, which are in agreement with each other. Furthermore, the *fit* method permits to discriminate different contributions by a direct fit on the histogram, while the *tag* method can be used to analyse and eventually extract common features of single events within the bursts.

Overall, the existence of bursts is an interesting phenomenon but it does not deteriorate the DUNE physics performance because even without applying any method to remove the bursts the rate of dark pulses is well below the DUNE DCR specification (200 Hz/mm^2 per sensor), as it is presented in table 5.

4.7 Time stability in liquid nitrogen

After the down-selection procedure, whose result is presented in the next section, a test to check the stability of one device in cryogenic condition was performed at Milano Bicocca University. A single SiPM was left in liquid nitrogen and powered to nominal over voltage of 3 V; dark noise was then measured continuously for 2 months. Test was performed in a dark room, with a clean environment for electromagnetic pickup, with all instruments connected after an UPS and electromagnetic filter. To further remove ambient light, SiPM was wrapped with teflon and black insulating tapes and an

2024 JINST 19 T01007

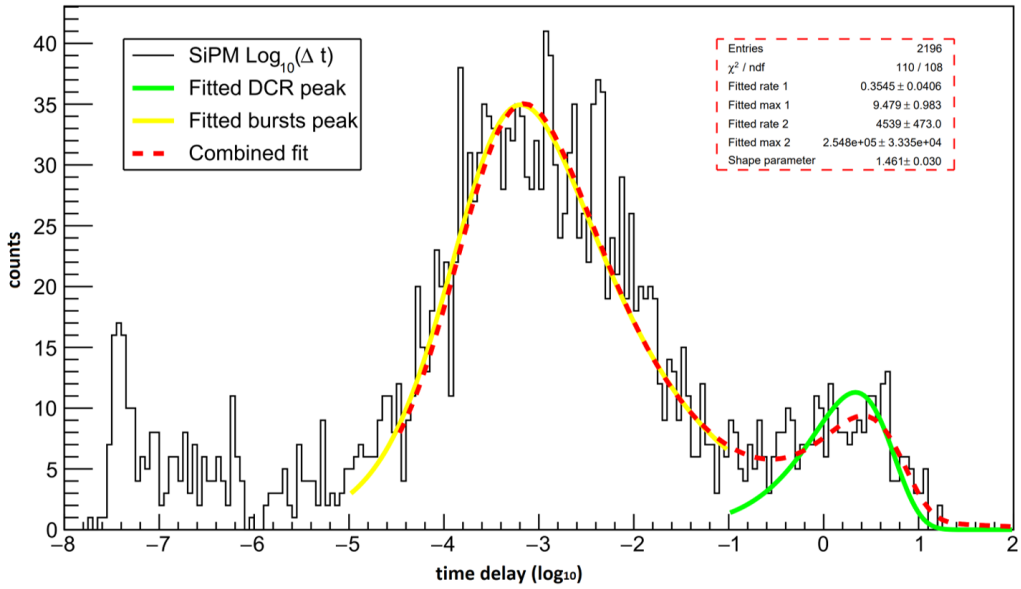

Figure 18. Histogram of the time interval (Δt) between consecutive peaks. Two different fits have been applied to the distribution: one for the DCR peaks (green solid line) and one for the burst peaks (yellow solid line). The dashed red line represents the combined fit of the two.

aluminum foil. The dewar was filled each week, to be sure that the SiPM is always covered by liquid nitrogen. No evidence of a dark noise increase over the time was found: the dark counts rate kept stable, with a min-max gap of 3.14 mHz/mm^2, after burst removal.

4.8 Summary of tests and results

The four prototypes were tested by the PDS Consortium in 2021 and the down-selection was completed in the fall of 2021. The tests were carried out with, first, a small-size production batch (25 SiPMs per model) to validate the prototypes before a larger production.

The tests described in table 4 were performed for all SiPMs belonging to the 25 SiPM batch. No thermal failures were reported and all prototypes met specifications. Thus we gave the green light to the production of the batches of 250 SiPMs for the four models and we performed the tests for all the SiPMs. A complete characterization of these sensors was performed to validate the thermal performance for a statistically significant set of SiPMs. All the data taken before and after 20 thermal cycles have shown no difference within the measurement experimental uncertainty. Table 5 reports the average values for the 250 SiPMs batch after the thermal cycles at 77 K (liquid nitrogen).

The PDS Consortium defined the criteria to down-select the prototypes as follows: best performance in gain, cross-talk, after-pulse and DCR at 77 K. The output is a figure of merit (FoM) given by the product of correlated noise (cross-talk + after pulse) times the DCR divided by the gain. The down-selected sensor is the sensor with minimum FoM among the tested prototypes.

Inspection of tables 5 and 6 shows a clear advantage of large cell-pitch sensors because of their higher gain, which is confirmed by the FoM. The minimum FoM is achieved by 75 µm HQR and therefore this has been the selected model. Finally, table 7 summarizes the measurement results for the selected model versus the values specified on the low level requirements for the SiPMs down-selection.

2024 JINST 19 T01007

Table 4. Summary of tests and the labs involved.

Test	Precision	Labs	Notes
Thermal tests		All: Bologna, Ferrara, CIEMAT, Prague, Milano-Bicocca and Valencia	All tests were performed before and after 20 thermal cycles for both, the 25 and 250 SiPM lots
Gain	10%	All	Precision limited by the calibration of the cold amplifier
Dark Count Rate	10-50%	All	Precision limited by the light tightness of the test-stand
Cross talk (%)	0.5% (absolute value)	All	Precision limited by the peak resolution in the waveform
After pulse (%)	0.5% (absolute value)	All	Precision limited by the peak resolution in the waveform
Non accelerated aging	2 months for down-selected only	Milano-Bicocca	2 months in LAr + accelerated aging in LN2. No effects reported
Accelerated aging		All	Equivalent to thermal tests
Ganging tests (SNR)		CIEMAT, Milano-Bicocca Milano-Statale	Limited by electromagnetic enviromental noise

Table 5. Averaged values per model after the thermal cycling. DCR+B stands for total DCR (including burst events), while for DCR-B, burst component is subtracted.

SiPM		Gain		DCR+B (mHz/mm^2)		DCR-B (mHz/mm^2)		Xtalk (%)		Afterpulses (%)	
Model	PDE (%)	Mean	Std Dev	Mean	Std Dev	Mean	Std Dev	Mean	Std Dev	Mean	Std Dev
50_LQR	40	2.55E+06	0.05E+06	51	14	17	7	10	3	1.1	0.5
	45	3.28E+06	0.04E+06	41	14	16	6	11	3	1.5	0.3
	50	4.01E+06	0.03E+06	48	15	18	7	13.7	1.8	2.0	0.6
50_HQR	40	2.51E+06	0.04E+06	84	13	22	4	8.1	0.9	1.5	0.5
	45	3.29E+06	0.04E+06	93	19	28	5	10.4	0.7	2.3	0.6
	50	4.06E+06	0.03E+06	118	10	41	6	11.2	0.7	2.5	0.6
75_LQR	40	3.78E+06	0.02E+06	90	40	25	7	11	3	0.5	0.2
	45	4.69E+06	0.02E+06	80	40	33	14	11.0	0.3	0.8	0.2
	50	5.59E+06	0.02E+06	90	40	33	11	12.9	1.0	1.1	0.3
75_HQR	40	3.93E+06	0.09E+06	58	11	28	10	6.6	0.7	0.9	0.2
	45	4.83E+06	0.09E+06	65	18	26	7	9.0	1.0	1.1	0.4
	50	5.70E+06	0.09E+06	55	17	30	9	11.0	1.0	1.3	0.3

5 SiPM ganging results

Scintillation light in each SuperCell is detected by 48 SiPMs, $6 \times 6\,\mathrm{mm}^2$ each. They are connected in parallel ("ganged") in subgroups of 6, and then 8 subgroups are connected in parallel at the inputs of the cold amplifier. A simplified diagram of the readout scheme is shown in figure 19. The same

2024 JINST 19 T01007

Table 6. Figure of Merit results.

Model	PDE (%)	FoM
50_LQR	40	3.08
	45	2.54
	50	2.80
50_HQR	40	3.18
	45	3.55
	50	3.98
75_LQR	40	2.64
	45	2.09
	50	2.36
75_HQR	40	1.15
	45	1.42
	50	1.49

Table 7. Summary of the selected SiPM (75 µm HQR) characteristics at 50% PDE (Vop = V_{bd} + 3 V) and comparison with the specific requirements.

Parameter	Requirement	Test Result (Mean/Std Dev)
Gain	2 to $8 \cdot 10^6$	$5.7 \cdot 10^6/9.08 \cdot 10^4$
Cross-talk probability	< 35% at Vop	13.62%/1.29%
After-pulsing probability	< 5% at Vop	1.49%/0.35%
Global DCR	< 100 mHz/mm^2	73.68 mHz/mm^2/26.6 mHz/mm^2
Thermal cycles	> 20	Negligible variation on V_{bd} R_q after 20 cycles

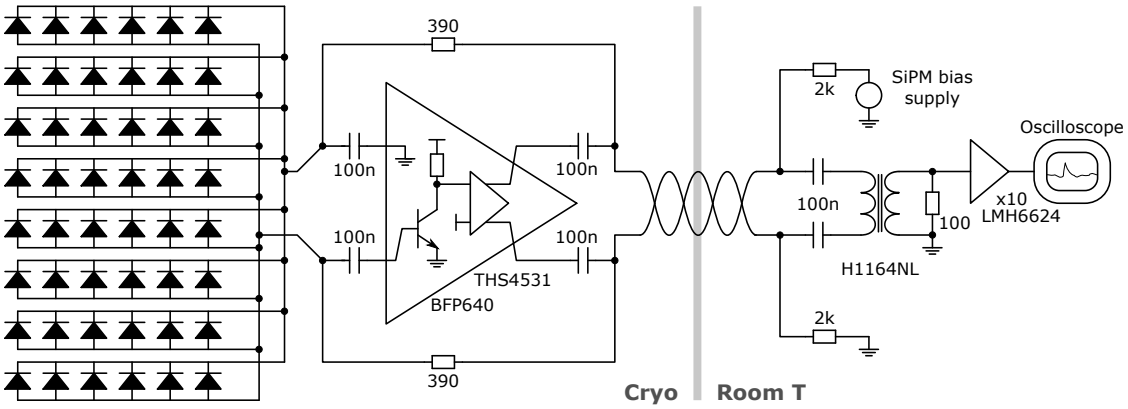

Figure 19. Simplified diagram of the ganging scheme.

twisted pair of wires are used to carry the SiPM bias voltage in DC and the differential output signals in AC. They are separated at the warm receiving end, where signals are converted to single-ended by

2024 JINST 19 T01007

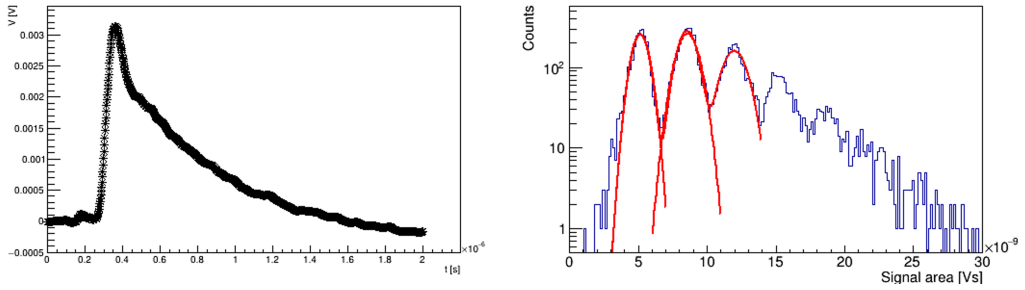

Figure 20. Left: averaged single photoelectron waveform and right: photoelectron spectra obtained reading out 48 HQR 75 µm. Measurements are taken at 45% of PDE, 4 V OV. The peaks corresponding to 0, 1, 2 photoelectrons were fitted with Gaussian functions.

Table 8. SNR measured for ganging of the various SiPM models, at 40%, 45% and 50% PDE. SNR is here defined as G/σ_1, where G is the gain and σ_1 is the width of the first photoelectron peak.

SNR	HQR 50 µm	HQR 75 µm	LQR 50 µm	LQR 75 µm
40%	4.68	5.21	6.79	3.77
45%	5.67	5.96	7.88	4.76
50%	6.57	6.66	8.29	5.76

a H1164NL transformer, amplified by a LMH6624 opamp with a gain of 10, and acquired at the oscilloscope. The low voltage supplies for the amplifier are provided by a different set of wires, not shown in the diagram.

The total capacitance at the input of the cold amplifier is about 60 nF. At such large value of capacitance, the signal to noise ratio (SNR) is dominated by the series voltage noise of the cold amplifier. A discrete-components design based on a SiGe heterojunction bipolar input transistor (BFP640) followed by a fully differential opamp (THS4531) was chosen. It gives a series white noise of $0.4\,\mathrm{nV}/\sqrt{\mathrm{Hz}}$ at a power consumption of about 2 mW (0.6 mA total current from a single 3.3 V supply). The closed-loop bandwidth is about 5 MHz, resulting in a typical signal rise time of 70 ns. The signal fall time is instead given by the recovery time of the SiPM cells. An undershoot is seen in the average signals due to the AC coupling at the outputs of the cold amplifier. The design of the cold amplifier is described in deeper detail in [6] and [12]. The same amplifier is used to test, in LN2, the ganging of 48 SiPMs of the four candidate Hamamatsu. The waveforms are collected by an oscilloscope and then analyzed in the same way as for gain measurements (see figure 20).

Measurements are taken at 40%, 45% and 50% of PDE. As reference V_{bd}, the mean V_{bd} of all the SiPM under test is used. The SNR values obtained with the various models are given in table 8, and the HQR 75 µm SiPM model shows a SNR > 4 for all V_{bd}. SNR is here defined as G/σ_1, where G is the gain and σ_1 is the width of the first photoelectron peak. The width of the first peak can be described as $\sigma_1 = \sigma_0 \oplus \sigma_{\mathrm{gain}}$, where σ_0 is the amplitude of the pedestal (the width of the electronic noise) and σ_{gain} corresponds to the additional spread of the first peak due to gain fluctuations between SiPMs. These are generated because all 48 SiPMs are biased at a given over-voltage above their average breakdown voltage, thus increasing the width of the single p.e. signal. With this definition, both effects over the PDS performance are being considered.

2024 JINST 19 T01007

A separate set of tests in LN2 was performed by the Milano Statale group at LASA (Laboratorio Acceleratori e Superconduttività Applicata — Laboratory for Accelerators and Applied Superconductivity), with the goal of validating the performance of the sensors in a configuration closer to the actual experimental one. From an implementation point-of-view, the sensors are grouped in 6 and installed on custom-designed SiPM Mounting Boards (SMB, figure 2 bottom) and then connected on 1 meter-long Signal Routing Boards (SRB) where each group of six is ganged together and the signal is routed to the cold amplifier [13].

In a first phase, the uniformity of response along the whole length of the SRB was verified by installing on it 8 fully equipped SMBs. The analysis of gain and signal shapes across all SMBs confirmed such uniformity of response, thus validating the design of Mounting and Routing Boards.

In a second phase, a half optical module (2 X-ARAPUCA supercells) was instrumented (but for the dichroic filters) and installed in an open Dewar filled with LN2. This set-up served as a test bench for the module integration, from the mechanical and electrical point of view, at cryogenic temperature (77 K).

The half-module was then read-out with a warm front-end, mimicking the analog stage of the DAQ, through a $\sim$ 30 m long Cat6 cable. The cable was immersed in LN2 as well, thus simulating signal transmission in the actual conditions of the first DUNE FD-HD. The two supercells comprising the half-module were then read-out independently, and waveforms were digitized with a Teledyne Lecroy HDO6104A oscilloscope. An optical fiber located on the top of the Dewar serves as illumination source, being connected to laser that provides the trigger signal to the oscilloscope.

Various HPK SiPMs were installed and tested in the half-module, performing scans in bias voltage and light intensity. In particular, the down-selected SiPMs (HPK 75 µm-HQR) were extensively characterized in this realistic environment. Measurements of SNR confirm that the selected sensors meet the technical requirements for the first DUNE FD-HD, in a configuration very close to the actual experimental one.

6 Conclusions

As described in previous sections, the HPK SiPM model selected to be used in DUNE FD1 PDS is the HQR 75 µm. It is clear that, both the signal to noise and gain are better for the larger pitch SiPMs than smaller pitch at same PDE, without a significant increment of dark current or correlated noise. Indeed, this model has the lowest level of correlated noise among the four models, mainly due to its high quenching resistance. In addition, its performance in the ganging configuration (the one to be used in the X-ARAPUCA technology) fulfills DUNE SNR requirements and ensures a larger dynamic range.

Beyond the needs of FD1-HD PDS, these results are interesting from a broader perspective and may be of value for dark matter and other neutrino experiments. The DUNE PDS Consortium has asked HPK to increase the quenching resistance of its commercial products to solve a well-known issue: a higher resistance (or, equivalently, a higher recharge time) mitigates the appearance of fast afterpulses, whose amplitude is comparable to single photoelectrons. All DUNE HPK prototypes solve this outstanding issue. The DUNE DCR requirements are not too stringent because the single photo-electron rate will be dominated by radiogenic background (^{39}Ar) and achieving the smallest possible DCR is not a critical requirement. On the other hand, small DCR values are interesting for experiments working with depleted argon or tighter radiogenic constraints (a field of interest for a

2024 JINST 19 T01007

possible future DUNE module). In this framework, a full understanding of the DCR burst origin and the optimal die field design may be worth an additional investigation.

Acknowledgments

The present research has been supported and partially funded by the Italian Ministero dell'Università e della Ricerca (PRIN 2017KC8WMB), by the Istituto Nazionale di Fisica Nucleare (experiment NU@FNAL), by the University of Ferrara (FIR2020), by the Fundación 'La Caixa', MICINN, Conselleria d'Innovació, Universitats, Ciència i Societat Digital, by the European Union's Horizon 2020 Research and Innovation programme under Grant Agreement No. 101004761, by European Union-Next Generation EU, by MCIN/AEI/10.13039/501100011033 under Grants No. PID2019-104676GB-C31 and RYC2021-031667-I of Spain, and by the Ministry of Education, Youth and Sports of the Czech Republic under the projects LM2018113 and LTT18001.

A special thanks to the workshop staff of the Istituto Nazionale di Fisica Nucleare of the Sezione di Bologna, in particular to Anselmo Margotti, Giulio Pancaldi, Andrea Zucchini, and of the Sezione di Ferrara, namely Alessandro Saputi, Michele Cavallina and Stefano Squerzanti.

This paper is dedicated to our friend and colleague Milos Lokajicek (1952–2023).

References

[1] DUNE collaboration, *Deep Underground Neutrino Experiment (DUNE), Far Detector Technical Design Report, Volume I Introduction to DUNE*, 2020 *JINST* **15** T08008 [arXiv:2002.02967].

[2] T. Heindl et al., *The scintillation of liquid argon*, *EPL* **91** (2010) 62002 [arXiv:1511.07718].

[3] H.V. Souza et al., *Liquid argon characterization of the X-ARAPUCA with alpha particles, gamma rays and cosmic muons*, 2021 *JINST* **16** P11002 [arXiv:2106.04505].

[4] DUNE collaboration, *Design, construction and operation of the ProtoDUNE-SP Liquid Argon TPC*, 2022 *JINST* **17** P01005 [arXiv:2108.01902].

[5] DUNE collaboration, *Deep Underground Neutrino Experiment (DUNE), Far Detector Technical Design Report, Volume III: DUNE Far Detector Technical Coordination*, 2020 *JINST* **15** T08009 [arXiv:2002.03008].

[6] P. Carniti et al., *A low noise and low power cryogenic amplifier for single photoelectron sensitivity with large arrays of SiPMs*, 2020 *JINST* **15** P01008 [arXiv:1911.06562].

[7] DUNE collaboration, *Detection efficiency measurement and operational tests of the X-Arapuca for the first module of DUNE far detector*, 2023 *JINST* **18** C02064 [arXiv:2211.15503].

[8] A. Nepomuk Otte, D. Garcia, T. Nguyen and D. Purushotham, *Characterization of Three High Efficiency and Blue Sensitive Silicon Photomultipliers*, *Nucl. Instrum. Meth. A* **846** (2017) 106 [arXiv:1606.05186].

[9] G. Collazuol et al., *Studies of silicon photomultipliers at cryogenic temperatures*, *Nucl. Instrum. Meth. A* **628** (2011) 389.

[10] F. Acerbi et al., *Cryogenic Characterization of FBK HD Near-UV Sensitive SiPMs*, *IEEE Trans. Electron. Dev.* **64** (2016) 521 [arXiv:1610.01915].

[11] M. Guarise et al., *A newly observed phenomenon in the characterisation of SiPM at cryogenic temperature*, 2021 *JINST* **16** T10006.

2024 JINST 19 T01007

[12] C. Brizzolari et al., *Cryogenic front-end amplifier design for large SiPM arrays in the DUNE FD1-HD photon detection system*, 2022 *JINST* **17** P11017 [arXiv:2207.13616].

[13] N. Gallice et al., *Development of a design for SiPMs readout in cryogenic environment for large area photon detectors*, in the proceedings of the *IEEE International Instrumentation and Measurement Technology Conference*, Glasgow, U.K., 17–20 May 2021 [DOI:10.1109/i2mtc50364.2021.9459995].

2024 JINST 19 T01007